HHS Public Access

Author manuscript

Neuron. Author manuscript; available in PMC 2021 March 04.

Published in final edited form as:

Neuron. 2020 March 04; 105(5): 909–920.e5. doi:10.1016/j.neuron.2019.11.024.

Synergy of distinct dopamine projection populations in behavioral reinforcement

Gabriel Heymann[1], **Yong Sang Jo**[1,2], **Kathryn L. Reichard**[3], **Naomi McFarland**[1], **Charles Chavkin**[3], **Richard D. Palmiter**[4,5], **Marta E. Soden**[3], **Larry S. Zweifel**[1,3,*]

[1]Department of Psychiatry, University of Washington, Seattle, WA 98195, USA.

[2]Department of Psychology, Korea University, Seoul 02841, Republic of Korea

[3]Department of Pharmacology, University of Washington, Seattle, WA 98195, USA.

[4]Department of Biochemistry, University of Washington, Seattle, WA 98195, USA.

[5]Howard Hughes Medical Institute, University of Washington, Seattle, WA 98195, USA.

Summary

Dopamine neurons of the ventral tegmental area (VTA) regulate reward association and motivation. It remains unclear whether there are distinct dopamine populations to mediate these functions. Using mouse genetics, we isolated two populations of dopamine-producing VTA neurons with divergent projections to the nucleus accumbens (NAc) core and shell. Inhibition of VTA-core projecting neurons disrupted Pavlovian reward learning and activation of these cells promoted the acquisition of an instrumental response. VTA-shell projecting neurons did not regulate Pavlovian reward learning and could not facilitate acquisition of an instrumental response, but their activation could drive robust responding in a previously learned instrumental task. Both populations are activated simultaneously by cues, actions, and rewards and this co-activation is required for robust reinforcement of behavior. Thus, there are functionally distinct dopamine populations in the VTA for promoting motivation and reward association that operate on the same time scale to optimize behavioral reinforcement.

eTOC

Heymann et al., genetically isolate dopamine-producing neurons of the ventral tegmental area with differential projections to the nucleus accumbens core and shell. They demonstrate that these

[*]**correspondence**: larryz@uw.edu.
Lead contact: Larry S. Zweifel

Author contributions

G.H., M.E.S. and L.S.Z conceptualized the study, designed experiments, analyzed data and wrote the paper. Y.S.J. performed electrophysiology *in vivo* and analyzed data, K.R. performed slice voltammetry and analyzed data with support from C.C., N.M. analyzed data. R.D.P. generated *Tacr3-*, *Ntsr1-*, and *Crhr1-frtFLEX-Cre* mice. L.S.Z produced AAV vectors.

Supplemental Information

Supplemental Figures 1–7.

Declaration of interests: The authors declare no competing interests.

projection-specific populations contribute distinctly to reward association and motivation, and work cooperatively to optimize behavioral reinforcement.

Introduction

Dopamine neurons of the ventral midbrain facilitate reward association and provide a prediction error signal (Schultz et al., 1997) that updates previously established stimulus-response and response-outcome associations through the modulation of cortico-striatal plasticity (Horvitz, 2009). In addition to facilitating reward learning, dopamine neurons provide an incentive salience signal to promote motivated behavioral responses (Berridge and Robinson, 1998).

The majority of dopamine neurons of the VTA project to the ventral striatum, which is divided into two major subdivisions, the NAc core and NAc shell. Establishing the role of specific dopamine projections in reward learning and motivation has been a considerable challenge. While there is general agreement that the NAc core and shell play an important role in these processes, how dopamine release within these subdivisions contributes to these distinct functions remains a subject of debate (Di Chiara, 2002; Floresco, 2015; Kelley, 1999; Saddoris et al., 2013). It has been proposed that the NAc core plays an essential role in instrumental responding and the NAc shell in Pavlovian association (Di Chiara, 2002). It has also been proposed that the NAc core is critical for Pavlovian association and the NAc shell for the regulation of motivated responses and the maintenance of reward responding (Floresco, 2015; Kelley, 1999; Saddoris et al., 2013). It was recently demonstrated that activation of dopamine projections to the NAc core, but not the NAc shell, was sufficient to promote the development of a Pavlovian conditioned response (Saunders et al., 2018). However, it remains to be determined how activation of shell projecting dopamine neurons influences reward-related behavior and whether dopamine projections to the core and shell work independently, or cooperatively.

Neuropeptide-related genes are highly enriched in VTA dopamine neurons (Chung et al., 2017) and neuropeptides potently modulate the dopamine system (Borgland et al., 2010; Kalivas, 1985; Margolis et al., 2014; Tyree and de Lecea, 2017; Werkman et al., 2011). In other brain regions, neuropeptides are known to functionally segregate divergent circuits related to reward processing (Kim et al., 2017; Tyree and de Lecea). Based on these observations, we hypothesized that Cre-driver mouse lines in which Cre expression is under the control of different neuropeptide-associated genes would allow us to isolate dopamine projection populations with differential innervation of the NAc. This in turn would allow us to parse the function of dopamine innervation of the NAc core and shell in the regulation of learning and motivation. Here, we demonstrate that *Crhr1*-Cre and *Cck*-Cre mouse lines isolate dopamine producing neurons in the VTA that differentially project to the NAc core and NAc shell, respectively. We find that these genetically isolated dopamine subpopulations, with differential projections to the core and shell, facilitate either reward association or motivation. We further demonstrate that the co-activation of these populations is critical for maximizing reinforcement behavior.

Results

Genetic isolation of dopamine neurons with differential innervation of the NAc

To test whether neuropeptide-associated genes could be used to isolate dopamine projection neurons with differential innervation of the NAc, we obtained or generated Cre-driver lines for four neuropeptide receptors (*Oprk1*-Cre, *Ntsr1*-Cre, *Tacr3*-Cre, and *Crhr1*-Cre) and the neuropeptide cholecystokinin (*Cck*-Cre) (Cai et al., 2016; Sanford et al., 2017; Taniguchi et al., 2011). These designated lines were injected with an adeno-associated viral vector (AAV) containing a Cre-dependent expression cassette for yellow fluorescent protein (AAV1-FLEX-YFP) into the VTA. We observed virally labelled cells within the VTA (Figure 1A and B) in each of the lines. Anatomical analysis of the distribution of labelled cell bodies demonstrated significant differences in the locations of these cells within the subdivisions of the VTA for two lines, *Crhr1*-Cre and *Cck*-Cre (Figure 1C). Consistent with the ability of these lines to isolate dopamine-producing neurons, virally labelled cells showed a high degree of overlap with tyrosine hydroxylase (TH), the rate-limiting enzyme in dopamine production, with the highest degree of overlap observed in *Crhr1*-Cre and *Cck*-Cre lines (Figure 1D).

To determine the projection patterns of genetically isolated neurons of the VTA, Cre-driver lines were injected with an AAV containing a conditional expression cassette for the synaptic protein synaptophysin fused to GFP (Carter et al., 2013) (AAV1-FLEX-Synaptophysin-GFP; Figure 2A). Innervation of three subdivisions of the NAc, the NAc core, the lateral region of the NAc shell (shell l.) and the medial region of the NAc shell (shell m.) were quantified along the rostral, intermediate, and caudal extent of the structure (Figure 2B). Innervation density was normalized to the fluorescence intensity at the site of injection (VTA). $Oprk1_{VTA}$ and $Ntsr1_{VTA}$ neurons displayed broad projections to the ventral striatum (Figure 2C and D) similar to labeling all dopamine projections in dopamine transporter (DAT)-Cre mice (Supplemental Figure 1A). In contrast, $Tacr3_{VTA}$ neurons showed some differential innervation of the NAc subregions, with the highest innervation observed in the shell m. (Figure 2C and D). $Crhr1_{VTA}$ neurons innervated the core preferentially over the shell m. and l. (Figure 2C and D). Cck_{VTA} neurons showed a significant projection bias to the shell m. over the shell l. and core (Figure 2C and D). For the three lines that showed the greatest differential innervation ($Tacr3_{VTA}$, $Crhr1_{VTA}$, and Cck_{VTA}) this pattern was most consistent across the rostral, intermediate, and caudal extent of the NAc in $Crhr1_{VTA}$ and Cck_{VTA} neurons (Supplemental Figure 1B–D). Some projection biases were also observed in the amygdala, but only $Oprk1_{VTA}$, and to a lesser extent $Ntsr1_{VTA}$, neurons projected to the prefrontal cortex (PFC, Supplemental Figure 1E–G).

To confirm the differences in projections to the NAc that we observed in our mapping analysis, we performed fast-scan cyclic voltammetry (FSCV) to measure optically-evoked dopamine release in the NAc (Figure 2E and Supplemental Figure 2A) from the three lines with the greatest differential innervation: *Tacr3*-Cre, *Crhr1*-Cre, and *Cck*-Cre mice. Mice were injected with AAV vectors containing a conditional expression cassette for channel-rhodopsin (Boyden et al., 2005) fused to mCherry (AAV1-FLEX-ChR2-mCherry) and optically-evoked dopamine was measured in designated brain regions and normalized to the

peak dopamine signal. Consistent with synaptophysin-GFP projection analysis, we observed significant differences in dopamine release. *Crhr1*-Cre mice displayed release in the core but not the shell, and *Cck*-Cre mice displayed release in the shell but not the core. In contrast, *Tacr3*-Cre mice, which showed the least consistent innervation bias along the rostral-caudal extent of the NAc, did not display differences in dopamine release (Figure 2F).

In addition to dopamine release, dopamine-producing neurons have been shown to co-release glutamate (Stuber et al., 2010) and GABA (Kim et al., 2015; Tritsch et al., 2012). To establish whether isolated dopamine populations co-release these transmitters in an anatomically specified manner, we measured light-induced excitatory and inhibitory postsynaptic currents (Li-EPSCs and Li-IPSCs) in subdivisions of the NAc (Supplemental Figure 2B and C). Consistent with our observation of differential dopamine release, we observed differential fast synaptic transmitter release in the NAc (Supplemental Figure 2D). $Crhr1_{VTA}$ neurons displayed predominantly inhibitory synaptic connections to the NAc core with no detectable connectivity in the shell (Supplemental Figure 2D). Cck_{VTA} displayed predominantly excitatory and feed-forward inhibitory connections in the shell m., predominantly inhibitory connections in the shell l. and no connectivity in the core (Supplemental Figure 2D). $Tacr3_{VTA}$ neurons showed predominantly excitatory and feed-forward inhibitory connections in the shell m. and sparse connectivity in the shell l. or core (Supplemental Figure 2D).

Based on the segregation of innervation of the shell and core by Cck_{VTA} and $Crhr1_{VTA}$ neurons, we performed RNAscope analysis to confirm differential expression of these markers in the VTA (Supplemental Figure 2E–J). We observed that 76.4% of *Cck* expressing neurons had no detectable expression of *Crhr1, and* an additional 8.6% had low levels of *Crhr1* transcript. Likewise, 75.4% of *Crhr1* expressing neurons had no detectable expression of *Cck*, an additional 10.7% had low levels of *Cck* transcript. VTA neurons with overlapping expression of both markers likely represent those cells with overlapping projections to the amygdala (Supplemental Figure 1F–G), as well as other minor projection targets.

We next asked whether isolated VTA neurons show differences in well-defined electrophysiological properties of dopamine cells. All three populations were sensitive to dopamine D2 autoreceptor-mediated inhibition, consistent with these neurons being dopaminergic (Supplemental Figure 3A–C). We observed no differences in a subset of intrinsic electrophysiological properties (Supplemental Figure 3D–M), consistent with previous observations of neurons projecting to the shell m. and core (Lammel et al., 2008). Based on the differential projections of Cck_{VTA} and $Crhr1_{VTA}$ neurons, their overlap with TH, differential dopamine release in the NAc, and D2 autoreceptor sensitivity, we will subsequently refer to these populations as VTA-shell and VTA-core projecting neurons, respectively.

Differential requirements of VTA populations for Pavlovian reward association

To establish necessity for VTA dopamine neurons with distinct projections to the core and shell for Pavlovian reward learning, we performed temporally-precise inhibition of VTA-shell and VTA-core projecting populations. The red light-shifted inhibitory opsin Jaws (Chuong et al., 2014) was conditionally expressed in either VTA-shell or VTA-core

projection neurons (AAV1-FLEX-Jaws-GFP, Figure 3a and Supplemental Figure 4A). Mice were trained in a simple Pavlovian conditioning paradigm in which two levers extended, followed 10 sec later by lever retraction (CS) that signaled food reward (20 mg sucrose pellet) delivery. VTA-shell and VTA-core neurons were bilaterally inhibited at the onset of the CS using a pulse of red light (2 sec on, followed by 1 sec ramp-down to prevent rebound excitation, Figure 3B) (Jo et al., 2018). Inhibition of VTA-core neurons resulted in a significant attenuation of head entry rate (head entries/min) during the CS compared to control mice expressing GFP that was similar to inhibiting the majority of VTA neurons in dopamine transporter (DAT)-Cre mice (Figure 3C). Inhibition of VTA-shell neurons did not affect CS-evoked head entry rate (Figure 3D). We did not observe significant differences in head entry rate relative to control mice during the inter-trial interval period (ITI, Supplemental Figure 4B). Disruption of Pavlovian reward learning associated with inhibition of VTA-core projecting neurons was not associated with an aversive response in a real-time place avoidance (RTPA) assay; however, a place avoidance was observed following inhibition of the majority of dopamine-producing neurons in the DAT-Cre mouse line (Supplemental Figure 4C).

As evidenced in Figure 3C, mice display a conditioned approach to the food-hopper during the CS presentation consistent with these animals displaying goal-tracking behavior (Parker et al., 2010). Although mice do not typically approach the CS (lever-press), a behavior referred to as sign-tracking (Flagel et al., 2011), they will rapidly acquire an instrumental response for reward delivery following Pavlovian conditioning that reflects a type of autoshaping (Gore and Zweifel, 2013). To assess whether inhibition of VTA-core or VTA-shell dopamine neurons during Pavlovian conditioning is associated with impaired autoshaping, we assayed mice in a simple fixed ratio 1 (FR1) schedule of reinforcement following conditioning (Figure 3D). During this response contingent phase, when cells were not inhibited, *Crhr1*-Cre (VTA-core) and DAT-Cre mice showed significantly reduced lever pressing compared to controls indicating they had not formed a strong association between the lever and the reward, but these mice did successfully acquire instrumental responding after additional days of training (Figure 3E). *Cck*-Cre (VTA-shell) mice did not differ from controls (Figure 3E).

Differential roles of VTA populations in instrumental reinforcement

It has been previously shown that animals will perform ICOSS for activation of dopamine-producing neurons (Witten et al., 2011) or for optical stimulation of dopamine fibers over the NAc (Steinberg et al., 2014). To assess whether optical stimulation of VTA-shell or VTA-core neurons is sufficient to promote ICOSS, we injected *Cck*-Cre, *Crhr1*-Cre, or DAT-Cre mice with AAV1-FLEX-ChR2-mCherry or AAV1-FLEX-mCherry (control) and placed an optical fiber (OF) over the VTA (Figure 4A and Supplemental Figure 4D). To promote reward-seeking behavior, mice were calorie restricted to 85% baseline body weight before conditioning. Optogenetic stimulation (20 Hz, 5-ms pulse width, 3 s) was time-locked with a lever press in an FR1 schedule of reinforcement in which both levers in the instrumental chamber were active. Following a lever press, the lever retracted with simultaneous delivery of the optical stimulation and the lever re-extended 5s following stimulation onset (Figure 4B). Stimulation of dopamine neurons in DAT-Cre mice resulted in robust instrumental

responding (Figure 4C). Activation of VTA-core neurons facilitated the acquisition of a weak, but significant instrumental response (Figure 4D) and mice could distinguish between an active (light) and an inactive (no light) lever (Figure 4E). In contrast, stimulation of VTA-shell neurons did not promote the acquisition of ICOSS (Figure 4F).

It has been previously proposed that dopamine projections to the NAc shell are not responsible for learning, *per se*, but rather provide an incentive salience signal to promote engagement of the motor action (Kelley, 1999). To test this, calorie-restricted mice were trained on an FR1 schedule of reinforcement for food reward for 5 days before transitioning to 5 days of ICOSS (Figure 4G). Optically implanted *Crhr1*-Cre and *Cck*-Cre mice expressing ChR2 or mCherry learned to lever press for food reward equivalently (Figure 4H). Following the switch to ICOSS, in both VTA-core stimulated mice and controls there was a transient increase in lever pressing on day 1 of ICOSS that decreased over time (Figure 4H); however, this time course was not sufficient to facilitate a complete extinction of responding. In contrast, stimulation of VTA-shell projecting neurons in *Cck*-Cre mice resulted in increased operant responding following the switch to ICOSS that persisted across all 5 testing days (Figure 4H). Similar to *Crhr1*-Cre mice following the acquisition of ICOSS (Figure 4E), *Cck*-Cre mice could distinguish between an active (light) and inactive (no light) lever once ICOSS of VTA-shell neurons was established (Figure 4I).

Stimulation of VTA-shell neurons resulted in a level of responding that was higher than we observed during FR1 responding for food reward (Figure 4H). Based on this observation, we asked whether stimulation of either VTA-core or VTA-shell neurons is preferred over natural food reward in calorie-restricted mice. Optically implanted *Crhr1*-Cre and *Cck*-Cre mice (Supplemental Figure 4E) were trained to press either of two levers for food pellet delivery for 3 days, then one of the levers was switched to optical stimulation (Figure 4J). ICOSS of VTA-core neurons was significantly less preferred to food reward (Figure 4K), but ICOSS of VTA-shell neurons was significantly preferred over food (Figure 4L). Thus, although activation of VTA-shell neurons is not sufficient to promote acquisition of an instrumental response it is a stronger reinforcer for maintaining an instrumental response than food.

To assess whether ICOSS of VTA-core or VTA-shell neurons is sufficient to drive motivated behavioral responses, we measured lever pressing in a progressive ratio schedule of reinforcement task. Control and *Cck*-Cre mice were trained on FR1 for food for 5 days then switched to optical stimulation for 5 days to establish ICOSS in *Cck*-Cre mice prior to testing in progressive ratio. *Crhr1*-Cre mice we trained for 5 days on FR1 for optical stimulation prior to testing in progressive ratio. ICOSS of VTA-shell neurons resulted in a significantly higher progressive ratio breakpoint than ICOSS in controls or of VTA-core neurons (Figure 4M).

VTA projection neuron populations require dopamine for their function

To establish whether the ICOSS behaviors we observe are indeed dependent on dopamine signaling in the NAc, we repeated these assays in mice with injection of the mixed dopamine D1 and D2 receptor antagonist flupentixol (Flpx) into the NAc core or shell (Supplemental Figure 4F–G). *Crhr1*-Cre and *Cck*-Cre mice were injected with AAV1-FLEX-ChR2-mCherry into the VTA and optically cannulated. A second infusion cannula was placed over

the NAc core (*Crhr1*-Cre mice, Figure 5A and Supplemental Figure 4F) or the NAc shell (*Cck*-Cre mice, Figure 5B and Supplemental Figure 4G). *Crhr1*-Cre mice were conditioned on an FR1 schedule for optical stimulation as above and either saline or Flpx (1μg) was infused 30 minutes prior to conditioning. Antagonizing dopamine signaling in the NAc core blocked the acquisition of ICOSS in these mice (Figure 5A). *Cck*-Cre mice were conditioned on an FR1 schedule for food for 5 days followed by optical stimulation for 5 days as above and either saline or Flpx (1μg) was infused 30 minutes prior to conditioning with optical stimulation. Antagonizing dopamine signaling in the NAc shell blocked the ICOSS observed in these mice following food reward conditioning (Figure 5B).

Antagonism of dopamine signaling in the NAc demonstrates that this structure is necessary for the observed behaviors, but does not directly demonstrate that dopamine release from VTA-core neurons expressing *Crhr1*-Cre and VTA-shell neurons expressing *Cck*-Cre is essential. To address this, we selectively inactivated the *Th* allele that is necessary for dopamine production in these populations. A major limitation to a conventional Cre-dependent gene inactivation approach is that *Crhr1* is expressed in TH neurons of the locus coeruleus (LC) (Valentino et al., 2012). Thus a *Crhr1-Cre::Th*$^{lox/lox}$ mouse would have a loss of TH in both VTA and LC neurons that could confound interpretations of behavioral data. To circumvent this problem, we generated a Flp recombinase-dependent *Crhr1* Cre line (*Crhr1-frtFLEX-Cre*, Figure 5C and Supplemental Figure 5A–C). Injection of AAV1-Flp-dsRed into the VTA results in activation of Cre recombinase (Supplemental Figure 5D) and subsequent inactivation of the floxed *Th* allele (Figure 5C). *Crhr1-frtFLEX-Cre* mice were crossed to *Th*$^{lox/lox}$ mice (Darvas et al., 2014) to generate *Crhr1-frtFLEX-Cre::Th*$^{lox/lox}$ and *Crhr1-frtFLEX-Cre::Th*$^{lox/+}$ mice. Injection of AAV1-FlpO together with AAV1-FLEX-ChR2mCherry allows for *Th* inactivation and ChR2 expression in *Crhr1*$_{VTA}$ neurons (Figure 5D and E and Supplemental Figure 5E). Selective elimination of dopamine synthesis in *Crhr1*-expressing neurons abolished the acquisition of ICOSS (Figure 5F).

Unlike *Crhr1*, *Cck* is not known to overlap with *Th* expression in other brain regions (Bolam and Smith, 1990; Lein et al. 2007). Thus, *Cck*-Cre mice were crossed with *Th*$^{lox/lox}$ mice to generate *Cck*-Cre::*Th*$^{lox/lox}$ and *Cck*-Cre::*Th*$^{lox+/}$ mice and ChR2 was conditionally expressed in these neurons (Figure 5G). TH immunoreactivity was eliminated from *Cck* neurons in the VTA but did not alter expression in *Th*-positive neurons in the LC (Figure 5H and Supplemental Figure 5F). Inactivation of *Th* in *Cck*$_{VTA}$ neurons significantly diminished instrumental responding after switching from food reward to ICOSS (Figure 5I and Supplemental Figure 5G).

Reward coding by VTA projection neuron populations

VTA-core and VTA-shell projection neurons differentially regulate Pavlovian reward association and instrumental behavior. To determine whether these VTA populations differentially encode reward-related information, we performed tetrode recordings *in vivo* using the optical-tagging strategy (Cohen et al., 2012; Jo et al., 2018; Lima et al., 2009) in VTA-shell (*Cck*$_{VTA}$) and VTA-core (*Crhr1*$_{VTA}$) projection neurons, and compared them to the dopamine population as a whole using DAT-Cre mice (Figure 6A and B and Supplemental Figure 6A). Mice were injected with AAV1-FLEX-ChR2 and implanted with

optrodes over the VTA (Figure 6A). Neuronal activity was recorded during instrumental conditioning with a FR1 schedule of reinforcement. Similar to ICOSS, the instrumental conditioning consisted of three events: lever extension which served as an auditory and visual cue indicating the start of the trial, lever press (action), and head entry to retrieve the food pellet reward (Figure 6A). After two days of pre-conditioning to establish a minimal level of responding for isolating reward-responsive units in implanted mice, we identified neurons based on their optical sensitivity. Optical sensitivity was established by presentation of 10 pulses of blue light (5 ms duration) at 20Hz for 10-stimulus sweeps (100 total stimulations/cell). Neurons were designated as light sensitive if they had an average spike latency ≤ 8 ms and a spike probability ≥ 0.6 (Figure 6B, Supplemental Figure 6B–C). Optrodes were lowered each day and optical sensitivity was assessed at the end of each conditioning session. In total, we identified 302 light-sensitive neurons during the 10 days of instrumental behavior (*Crhr1*-Cre, n=4 mice, N=100 cells; *Cck*-Cre, n=3 mice, N=117 cells; DAT-Cre, n=3 mice, N=85 cells). We did not observe significant differences in the average action potential waveform of optically sensitive neurons between the three groups (Figure 6A). Basic electrophysiological properties of light-sensitive neurons did not differ between groups (Supplemental Figure 6D–F) and these properties did not differ between groups during the early (Supplemental Figure 6G–H) or late phases of conditioning (Supplemental Figure 6J–L).

All three groups of mice acquired instrumental responding to the FR1 schedule of reinforcement equivalently (Figure 6C). Across all ten days of conditioning, we observed time-locked responses to the three events (cue, action, and reward) in all three groups of mice (Fig 6d and Supplemental Figure 6M–O). Average phasic activation of cells responsive to the designated events across conditioning days was not different between groups (Figure 6D) and these responses did not differ during early or late phase of conditioning (Supplemental Figure 6P–Q). Consistent with these observations, identification of cells using a more stringent selection criterion (Cohen et al., 2012) (≥0.9 spike probability and ≤ 5 ms spike latency) yielded similar response profiles (Supplemental Figure 6R–S).

We did not observe differences between the groups in the proportions of cells that responded to the cue or the action (Fig 6D). However, we did observe significant differences in the proportion of cells that responded to the reward (Figure 6D), with DAT-Cre and *Cck*-Cre mice displaying a significant negative correlation between the proportion of reward-responsive cells and conditioning day (Figure 6E).

Synergistic action of distinct VTA projection populations

VTA-core and VTA-shell projecting dopamine neurons are activated to a similar degree during instrumental conditioning, consistent with previous reports of simultaneous dopamine release in the core and shell (Saddoris et al., 2015). Our ability to isolate dopamine neurons with differential innervation of the NAc core and shell allowed us to address whether the simultaneous activation of neurons projecting to these regions is necessary to drive robust behavioral responses through coincident signals for reward association and motivation (Figure 7A). To achieve this, we generated double transgenic *Crhr1*-Cre::*Cck*-Cre mice (Figure 7B and Supplemental Figure 7A) and assayed their behavior in an FR1 schedule of

reinforcement for ICOSS of both populations. We observed robust self-stimulation in these mice (Figure 7B) and the emergence of a real-time place preference (RTPP, Figure 7C) that was not observed when these populations were stimulated independently (Supplemental Figure 7B).

It is possible that the observed behavior in the double transgenic *Crhr1*-Cre::*Cck*-Cre mice is simply a reflection of increasing the total number of neurons stimulated and is independent of the now combined projections of these neurons to the NAc core and NAc shell. Indeed, these neurons each represent approximately half of the overall dopamine neuron population (Figure 7D). If this is true, then optical activation of a genetically isolated population of dopamine producing neurons that has projections to both the NAc core and the NAc shell but represents less than half of the total dopamine population should not be reinforcing. Conveniently, $Tacr3_{VTA}$ neurons have a strong projection to the shell, have some projections to the core (Figure 2D–G and Supplemental Figure 3C), and represent approximately one-third of the total dopamine population (Figure 7D). Activation of $Tacr3_{VTA}$ neurons (Supplemental Figure 12A) was as effective at promoting ICOSS as *Crhr1*-Cre::*Cck*-Cre double transgenic mice (Figure 7B) and was sufficient to elicit an RTPP (Figure 7C).

Discussion

Genetic isolation of VTA dopamine populations

Using a genetic strategy in mice, we were able to isolate VTA populations with differential projections to the NAc and demonstrate that these populations mediate distinct functions, but work synergistically to promote robust behavioral reinforcement. Genetic diversity in dopamine projection populations has recently been demonstrated (Poulin et al., 2018). Utilizing a candidate gene approach based on neuropeptide-related gene expression, we were also able to resolve projection-specific VTA populations. Consistent with our observed differential innervation, we observed differential dopamine release from these populations in the NAc core and NAc shell.

Cck_{VTA} projections have been described previously (Poulin et al., 2018) where it was observed that these neurons differentially innervate the NAc, though in that case they observed a slightly larger projection to the Core than we report here. The reason for this difference is unclear, but it may reflect the sensitivity of the assays used to measure this projection. Here we used both fluorescent labeling of this projection through the expression of GFP-fused to the synaptic marker synaptophysin, measured light-evoked dopamine release using FSCV, and measured light-evoked IPSCs and EPSCs, in all three cases we observed little connectivity between Cck_{VTA} neurons and the NAc core.

In addition to dopamine neurons that co-release these neurotransmitters, there are many cells within the VTA that are non-dopamine glutamate and GABA releasing (Morales and Margolis, 2017). These neurotransmitter systems have also been shown to play important roles in the regulation of behavior. For example, activation of glutamate neurons of the VTA has been shown to be rewarding in a dopamine-independent manner (Yoo et al., 2016). Intriguingly, activation of glutamate projections from the VTA to NAc alone was found to be aversive (Qi et al., 2016). GABA projections to the NAc have also been shown to promote

reinforcement learning (Brown et al., 2012). Although we observed glutamate release from *Cck*-Cre expressing neurons in the NAc Shell and GABA release in the NAc core from *Crhr1*-Cre expressing neurons, the behavioral effects observed are prevented by the genetic inactivation of dopamine production by these neurons indicating dopamine is the principal neurotransmitter in driving the observed behavior.

It is not fully resolved what the function of the neuropeptides and neuropeptides receptors expressed by dopamine neurons is relative to their roles in reward association and motivation. We also do not have a full appreciation of where all of the neuropeptide inputs to the VTA come from. Future studies designed to elucidate the pathway-specific roles of these modulators will be greatly facilitated by the numerous Cre-driver lines, intersectional Cre-driver lines such as the *Crhr1*-frtFLEX-Cre line described here, cell type-specific gene inactivation strategies (Yamaguchi et al., 2018), advanced cell-specific retrograde tracing methods (Chatterjee et al., 2018; Sanford et al., 2017), and neuropeptide-specific sensors (Patriarchi et al., 2018; Stoeber et al., 2018) that are rapidly emerging.

Reward coding by VTA dopamine populations

We find that the response profiles of dopamine neurons with different projections are largely indistinguishable during early and late phases of conditioning. One caveat to this observation is that we had to condition the mice for two days to get a sufficient number of responses (>10 lever presses) to perform our analysis; thus, it is possible we missed differences in these populations in this earliest phase. However, because mice steadily increased the number of lever presses across the first 6 days until reaching asymptotic performance on days 7–10, it is unlikely that we missed significant differences in these populations during the acquisition phase.

Previous studies have demonstrated differential dopamine release patterns in the NAc core and NAc shell in response to distinct phases of reinforcement (Saddoris et al., 2015) that is inconsistent with the largely indistinguishable patterns of action potential firing we observe here. However, recent data suggests that the terminal dopamine release does not always directly reflect the action potential firing patterns of the dopamine neurons, and it was proposed that postsynaptic modulation of dopamine release dynamics in distinct subdivisions of the NAc endow the behavioral specificity of dopamine release in these areas (Berke, 2018; Mohebi et al., 2019).

Synergy of VTA dopamine populations

Through the isolation of dopamine neurons that innervate either the NAc core or shell, we were able to demonstrate that VTA dopamine-producing neurons that innervate the NAc core facilitate the acquisition of an instrumental response and Pavlovian reward association. These findings are consistent with a recent report using optogenetics to isolate distinct dopamine projections in the rat (Saunders et al., 2018). Saunders and colleagues demonstrated that optogenetic activation of dopamine projections to the NAc core was sufficient to instantiate a Pavlovian association with a conditioned stimulus. Intriguingly, they did not find an effect of optogenetic pairing of the CS with dopamine projections to the shell.

Optogenetic stimulation of VTA-core projecting neurons is sufficient to facilitate the acquisition of an instrumental response. In contrast, stimulation of VTA-shell projecting neurons was unable to facilitate the acquisition of an instrumental response *de novo*, but promoted a high level of responding if an association had been previously established. When activated simultaneously, these two populations promoted robust reinforcement behavior. Intriguingly, $Tacr3_{VTA}$ neurons that project to the NAc shell and to the NAc core are significantly fewer in number than either $Crhr1_{VTA}$ or Cck_{VTA} neurons, but are sufficient to promote robust instrumental responding. Thus, $Tacr3_{VTA}$ neurons appear to represent a minimally sufficient dopamine population for reward reinforcement.

Our results are consistent with the proposed framework in which dopamine regulation of ventral striatal function through distinct projections to the NAc core and shell coordinately regulate reinforcement of behavior (Kelley, 1999; Saddoris et al., 2013). It has been proposed that the NAc core, through its anatomical and structural similarity to the caudate (dorsal striatum) regulates motor learning (Kelley, 1999). Dopamine release in the NAc core facilitates NMDA receptor-dependent learning of the motor action(s) that led to the delivery of the reward (Kelley, 1999). The NAc shell is not responsible for learning, *per se*, but rather receives a *coincident* dopamine signal that provides incentive salience to promote engagement of the motor action (Kelley, 1999). In the context of this study, initial learning is facilitated by the activation of VTA-core projecting neurons to the primary reward to release dopamine in the core and reinforce the motor program that led to the acquisition of the reward. Concurrently, activation of VTA-shell projecting neurons releases dopamine in the shell to signal the motivation to perform the action.

STAR Methods

Lead Contact and Materials Availability

- Further information and requests for resources and reagents should be directed to and will be fulfilled by the Lead Contact, Larry Zweifel (larryz@uw.edu).
- All unique stable reagents generated in this study will be made available upon request but we may require a payment and/or Material Transfer Agreement if there is a potential for commercial application.

Experimental Model and Subject Details

Male and female mice were housed on a 12-hour light/dark cycle. All experiments were performed during the light phase under the guidelines of the Institutional Animal Care and Use Committee at the University of Washington. Mice were aged 2 – 5 months for behavioral analysis, 4–6 months for *in vivo* electrophysiology, 6 – 8 weeks for slice electrophysiological and 9 – 12 weeks for voltammetry experiments.

Method Details

Generation of Cre-driver mouse lines.—*Tacr3*-Cre mice were made by inserting a 4 kb 5’ arm and a 4.5 kb 3’ arm (each made by PCR amplification from a C57Bl/6 BAC clone with Q5 DNA polymerase and unique restriction sites at each end) into a targeting vector with *ires*-Cre*:GFP*, frt-flanked *SV-Neo* (for positive selection), *HSV-TK* and *Pgk-DTa* (for

negative selection). The targeting construct was electroporated in G4 (129/Sv × C57Bl/6 hybrid) embryonic stem cells. Correct gene targeting was detected in 5 of 77 clones by Southern blot using *EcoR*V and a radioactive probe outside the 5' arm. One of the clones gave high percentage chimeras and germline transmission. The SV-Neo gene was removed by a cross with *Gt(ROSA)26Sor-FLP* recombinase and then *Tacr3*-Cre mice (identified using a 3-primer PCR strategy) were continuously backcrossed to C57Bl/6 mice.

Ntsr1-frtFLEX-Cre mice were made by inserting a 5 kb 5' arm and a 5 kb 3' arm (PCR amplified from a C57Bl/6 BAC clone with Q5 DNA polymerase as above) into a targeting vector with a FLP recombinase-dependent Cre (*ires-frtFLEX-Cre:GFP)*, loxP-flanked *SV-Neo* for positive selection and *HSV-TK* and *Pgk-DTa* genes for negative selection. A FLP-dependent Cre recombinase was constructed by inserting a *Mt1* gene intron within the open reading frame of mnCre:GFP, which has a Myc tag (m), followed by a nuclear localization signal (NLS, n), followed by Cre recombinase fused to green fluorescent protein (Cre:GFP), to generate a gene with two exons. Then the second exon was inverted and flanked by a pair of dissimilar frt sites to make a double inverted orientation (DIO) construct (denoted as 'FLEX'). The action of FLP recombinase inverts the second exon thereby allowing splicing to generate functional Cre recombinase. The targeting construct was electroporated in G4 (129/Sv × C57Bl/6 hybrid) embryonic stem cells. Correct gene targeting was detected in 11 of 63 clones by Southern blot using *Bgl*II and a radioactive probe outside the 5' arm. One of the clones gave high percentage chimeras and germline transmission. The loxP-flanked SV-Neo gene was removed by a cross with *Meox*-Cre mice. The mice were bred with C57Bl/6 mice to remove the *Meox*-Cre gene and establish C57Bl/6 genetic background. *Ntsr1*-Cre mice were identified using a 3-primer PCR strategy.

Crhr1-frtFLEX-Cre were generated by inserting a 5.9 kb 5' arm and a 4 kb 3' arm (PCR amplified from a C57Bl/6 BAC clone with Q5 DNA polymerase as above) into a targeting vector with a FLP recombinase-dependent Cre (*ires-frtFLEX*-Cre*:GFP*, as above), loxP-flanked *SV-Neo* for positive selection), with *HSV-TK* and *Pgk-DTa* genes for negative selection. Correct gene targeting was detected in 23 of 42 clones by Southern blot using *EcoR*V and a radioactive probe outside the 5' arm. One of the clones gave high percentage chimeras and germline transmission. The loxP-flanked SV-Neo gene was removed by a cross with *Meox*-Cre mice. The mice were bred with C57Bl/6 mice to remove the *Meox*-Cre gene and establish C57Bl/6 genetic background. *Ntsr1-FLP*-Cre mice were identified using a 3-primer PCR strategy.

Viral production.—AAV viral vectors (serotype 1) were generated as previously described (Gore et al., 2013). Briefly, pAAV shuttle plasmids for ChR2-mCherry (pAAV-Ef1α-FLEX-ChR2-mCherry, mCherry (pAAV- Ef1α-FLEX-mCherry), Jaws (pAAV-CAG-FLEX-Jaws-GFP), YFP (pAAV- Ef1α-FLEX-YFP), and FlpO-dsRed (pAAV-CAG-FlpO-dsRed) were co-transfected with the packing plasmid pDG1 (Nature Biotechnologies) into HEK293T/17J cells (ATCC). 72 hours post-transfection cells were harvested and viral vector was liberated by repeated freeze/thaw. Vectors were purified by multiple rounds of cesium chloride gradient centrifugation, sucrose gradient centrifugation, and dialysis. Viral vectors were stereotaxically injected at a final titer of $1–3 \times 10^{12}$ particles/ml.

Surgery.—Mice were under constant anesthesia (1.5 – 4%) and head fixed in a stereotax (Model 1900, David Kopf Instruments). Coordinates were standardized to bregma and anterior-posterior positions were adjusted using a correction factor (F = Bregma – Lambda/4.21). The Hamilton injection syringe was lowered 0.5 mm past the indicated depth and 0.5 μl virus was injected at a rate of 0.25 μl/min as the syringe was raised to the desired depth. VTA coordinates (relative to bregma): × = +/−0.5 mm, y = −3.35 mm, z = −4.5 mm.

Characterizing Cre-line subpopulations in the VTA.—A Cre-conditional fluorescent reporter virus (AAV1-FLEX-YFP) was injected bilaterally into the VTA of *Oprk1*-Cre, *Ntsr1*-Cre, *Tacr3*-Cre, *Crhr1*-Cre or *Cck*-Cre mice. 3 wks following surgery, 30-μm sections were taken for the rostral-caudal extent of the VTA. One section per atlas image (Paxinos and Franklin, Figures 55–63) was selected and stained overnight with a Rabbit anti-GFP antibody (Invitrogen A11122, 1:2000). Sections were co-stained for tyrosine hydroxylase using a Mouse anti-TH antibody (Millipore MAB318, 1:1000). Images were collected at 10x magnification using a Keyence BZ-X710 fluorescent microscope and analyzed using ImageJ software. YFP-positive/TH-negative and YFP-positive/TH-positive cells were counted manually.

Mapping Cre-line subpopulation projections.—To characterize and quantify the projections of $Oprk1_{VTA}$, $Ntsr1_{VTA}$, $Tacr3_{VTA}$, $Crhr1_{VTA}$ or Cck_{VTA} populations, mice were injected with AAV1-DIO-synaptophysinGFP bilaterally into the VTA. ~3 weeks following surgery, mice were perfused and 30-μm coronal brain sections were collected for the entire brain and stained overnight with a Rabbit anti-GFP antibody (Invitrogen A11122, 1:2000). Every 6^{th} section (every 180 μm) was visually inspected for terminal GFP expression. Images were collected at 2x magnification using a Keyence BZ-X710 fluorescent microscope and analyzed using ImageJ software. Images were background subtracted and mean pixel intensity was measured. For striatal subregions, mean pixel density was normalized to the mean pixel density at the injection site in the VTA to yield relative density values.

Fast-scan cyclic slice voltammetry.—*Crhr1*-Cre, *Cck*-Cre and *Tacr3*-Cre mice (4 – 5 wk old) were injected bilaterally in the VTA with a Cre-conditional Channelrhodopsin virus (AAV1-FLEX-ChR2-mCherry). Approximately 3 wks post-surgery, mice were euthanized and decapitated. Brains were immediately submerged in ice-cold aCSF solution in which sucrose replaced NaCl. Coronal slices (250 μm) through the striatum were kept in oxygenated aCSF (in mM: 124 NaCl, 2.5 KCl, 1.25 NaH_2PO4, 2 $MgSO_4$, 2 $CaCl_2$, 10 glucose, and 26 $NaHCO_3$) at 37°C for an hour prior to recording. Slices were perfused with oxygenated aCSF at 31–33°C at 1.5–2.0 mL/min.

Dopamine release was recorded with a carbon fiber microelectrode (Clark et al., 2010). The potential at the recording electrode was held at −0.4V vs. an $Ag/AgCl_2$ reference electrode and ramped to +1.3V and back to −0.4V, with one triangular waveform cycle every 100 ms. Waveform generation and data acquisition were performed using software written in LabVIEW (National Instuments, TX). Recordings were performed in three locations per slice: nucleus accumbens medial shell, lateral shell, and core. Fluorescence was verified and imaged after recordings. Representative recordings were taken across the A-P axis from +1.5

to +0.7 from bregma. Dopamine release was evoked from ChR2-expressing terminals with a 3-s train (20 Hz, 5-ms pulse width) at 485 nm using the Spectra 4-LCR-XA (Lumencor) light source. Three stimulations were averaged to determine release from each subregion. For each section, measurements were normalized to the largest current amplitude evoked in the slice (from any of the 3 subregions).

Slice Electrophysiology.—Horizontal or coronal brain slices (200 or 250 μm, respectively) were prepared in an ice slush solution containing (in mM): 92 NMDG, 2.5 KCl, 1.25 NaH_2PO_4, 30 $NaHCO_3$, 20 HEPES, 25 glucose, 2 thiouria, 5 Na-ascorbate, 3 Na-pyruvate, 0.5 $CaCl_2$, 10 $MgSO_4$, pH 7.3–7.4 (Ting et al., 2014). Slices recovered for ≤12 minutes in the same solution at 32°C and then were transferred to a room temperature solution containing (in mM): 92 NaCl, 2.5 KCl, 1.25 NaH_2PO_4, 30 $NaHCO_3$, 20 HEPES, 25 glucose, 2 thiouria, 5 Na-ascorbate, 3 Na-pyruvate, 2 $CaCl_2$, 2 $MgSO_4$. Slices recovered for an additional 45 minutes before recordings were made in aCSF at 32°C continually perfused over slices at a rate of ~2 ml/min and containing (in mM): 126 NaCl, 2.5 KCl, 1.2 NaH2PO4, 1.2 MgCl2 11 D-glucose, 18 NaHCO3, 2.4 CaCl2. All solutions were continually bubbled with O_2/CO_2.

Whole-cell recordings were made using an Axopatch 700B amplifier (Molecular Devices) with filtering at 1 KHz using 4–6 MΩ electrodes. A Cre-conditional fluorescent reporter virus (AAV1-DIO-YFP) was used to identify *Crhr1*$_{VTA}$, *Cck*$_{VTA}$, or *Tacr3*$_{VTA}$ neurons for characterization of intrinsic properties. ~3 weeks following surgery, 200-μm horizontal brain slices of the VTA were prepared for recording. Electrodes were filled with internal solution containing (in mM): 130 K-Gluconate, 0.1 EGTA, 10 HEPES, 5 Mg-ATP, 0.5 Na-GTP, 5 NaCl, pH 7.3, 280 mOsm. Hyperpolarization-activated (Ih) current was evoked by a series of hyperpolarizing voltage steps from −70 to −80, −90, −100, −110 and −120 mV. Tail currents were evoked by repolarization to −60 mV following a 500-ms voltage step to 0 mV from a holding potential of −60 mV. The amplitude was calculated from the average of 5 sweeps. Baseline firing rate was recorded in current clamp mode. For a subset of cells with stable firing, Quinpirole (1 uM) was washed into the bath to assess D2 sensitivity. Resting membrane potential was also measured during current-clamp recordings.

For light-evoked EPSC and IPSC recordings of VTA outputs to nucleus accumbens subregions, *Crhr1*-Cre, *Cck*-Cre and *Tacr3*-Cre mice (4 – 5 weeks) were injected bilaterally in the VTA with a Cre-conditional Channelrhodopsin virus (AAV1-FLEX-ChR2-mCherry). ~3 weeks post-surgery, 250-μm coronal brain slices of the striatum were prepared for recording. Electrodes were filled with internal solution containing (in mM): 132 $CsMeSO_3$, 8 CsCl, 10 HEPES, 1 EGTA, 0.5 $CaCl_2$, 10 Glucose, 5 QX-314, pH 7.3, 280 mOsm. Light-evoked synaptic transmission was induced with 5-ms light pulses delivered at 0.1 Hz from an optic fiber placed directly in the bath. Light-evoked EPSCs were recorded while holding at −60 mV and IPSCs were recorded while holding at 0 mV. CNQX (10 μM) was applied to the bath solution to block excitatory and feed-forward inhibition responses. Picrotoxin (1 μM) was applied to block IPSCs. Amplitudes and example current traces represent an average of at least 10 events.

RNAscope in situ hybridization.—The RNAscope assay(Wang et al., 2012) was performed on Bl6 wild-type adult mice. Briefly, brains were quickly excised, flash frozen in 2-methylbutane, and stored at −80 degrees Celsius. 10-μm brain slices were prepared for the rostral, medial and caudal VTA for each animal. Sections were prepared for hybridization per manufacturer's (Advanced Cell Diagnostics, Inc) instructions using probes for *Crhr1* (Mm-*Crhr1*) and *Cck* (Mm-*Cck*-C3; 1:50 dilution). Slides were cover slipped and imaged using the Keyence BZ-X710 fluorescent microscope. Overlap was quantified for each section at 10x magnification using ImageJ software. Minimal detectable expression for each probe was established by drawing an ROI (8μm diameter) around cells with a visually detectable single puncta of signal corresponding to a single mRNA transcript (Advanced Cell Diagnostics, Inc). The mean pixel intensity of single transcript containing cells for each probe was measured from 10 cells per section. The range of mean pixel intensity for *Crhr1* was 2–6 and the mean pixel intensity range for *Cck* was 4–11; therefore a mean pixel intensity >2 was set for detection of *Crhr1* and >4 for *Cck*. All cells within the VTA with visibly detectable puncta were selected as an ROI bilaterally and the mean pixel intensity for the designated probe was measured along with the mean pixel intensity of the same ROI in the alternate channel containing signal for the other probe. This was performed using each probe as the primary signal detection and was quantified from three sections per mouse corresponding to one section from the rostral VTA, one section from the intermediate VTA, and one section from the caudal VTA.

In vivo physiology—A microdrive containing an optic fiber and four recording tetrodes (25 μm diameter tungsten wire; California Fine Wire) was implanted dorsal to the VTA (3.7 mm to the brain surface) after AAV-FLEX-ChR2-mCherry was infused (Gore et al., 2017; Jo and Mizumori, 2016). The distance between the fiber and tetrode tips was kept less than 500 μm. After recovery, each mouse was food-restricted to 85% and shaped to press a lever for a food pellet in an operant box for a food pellet for 2 days. After the habituation, the mouse was placed in a holding cage and single-unit activity was monitored using a Cheetah data acquisition system (Digital Lynx 4SX, Neuralynx). Neural signals were filtered between 0.6 and 6 kHz and digitized at 32 kHz. Unit spikes were recorded for 1 ms after voltage potentials exceeded a predetermined threshold at 500–7000X amplification. To identify ChR2-expressing neurons in the VTA, 10 blue light pulses (473 nm; 5-ms long at 20 Hz; Laserglow technologies) were presented via the optic fiber of the microdrive. The light intensity (5–15 mW/mm^2) was adjusted, so that light-evoked spike waveforms were similar to spontaneous ones. Stimulations were repeated for 10 sweeps of 10 light pulses for total of 100 presentations. Light-responsive cells were designated based on the analysis of the distribution of the average latency of responding to the light pulse and the distribution of the average probability of spike firing. There was a natural separation of the distribution at 8 ms latency and 0.6 probability. Cell meeting both criterion (<8 ms latency and >06 probability) were designated responsive. These cells also showed high correlations between spontaneous and light-evoked waveforms. The waveform correlations were calculated between spontaneous spikes and light-evoked signals recorded from continuous sampled channels single recording day. Light sensitivity and waveform correlations were performed for each recording day. Once light-responsive units were found, the mouse underwent 10 daily recording sessions. In each session, neuronal responses to the light pulses were first recorded

in the holding cage. Then basal firing patterns were measured in the operant box for 10 min. Then the behavioral recording was conducted for 1 hour. After the recording session, all tetrodes were lowered in 80 μm increments to find different light-responsive units. If no light-responsive units were observed on a given day, the tetrodes were moved down until new light-responsive units were encountered. These neuronal responses during the operant conditioning were recorded on the following day.

To analyze the unit data, single units were isolated based on various waveform features using an Offline Sorter (Plexon). Only units showing good recording stability throughout the whole recording session were included for further analysis. These neuronal responses to the cue, action, and reward during the operant conditioning were examined with peri-event time histograms (PETHs; 50-ms bins) constructed around the times of the three events. Firing rates in PETHs were transformed to z-scores relative to basal firing rates during the 10 min recording period prior to the operant conditioning. A VTA cell was classified as responsive to each event if its average z-score during each event period (cue, 0 to 300 ms; action, −100 to 200 ms; reward, −50 to 350 ms) was greater than 2.5. This designation was set based on a conservative estimate given that a z-score greater than 2.2 has a Bonferroni corrected P value < 0.017. The designation of the time window for assessing responsiveness was based on the fact that the mice are freely moving. To account for trial to trial variability in proximity to the cue and based on visual inspection of PETHs related to cue presentation, the cue-responsive window was set from 0 (cue onset) to 300 ms to maximize detection of responsive units. To account slight time variability from initiation of the lever press to the completion of the lever press and to account for observed increases in activity just prior the action completion based on visual inspection of PETHs the action responsiveness was set between −100 from lever press to 200 ms after lever press. Similarly to account for variability in time differences between head entry into the food pellet delivery port and actual oral grasping of the reward pellet the time window was set to −50 ms prior to beam break designating head entry and 350 ms after beam break.

Optogenetic excitation/inhibition and reinforcement conditioning paradigms.

—For activation of VTA subpopulations, AAV1-FLEX-ChR2-mCherry was injected unilaterally into the VTA of adult mice. A custom-built optic fiber cannula was implanted 0.5 mm dorsal to the injection site and affixed to the skull with Metabond and dental cement. Only optic fibers with > 70% power retention were used. For all experiments (except real-time place preference), mice were maintained at 85 – 90 % of baseline body weight starting 1 week prior to experimentation. All operant and Pavlovian conditioning assays were performed in Med Associates Inc. behavior boxes. Each behavior box had 2 levers positioned on either side of a food hopper on one wall, with a house light centered on the opposite wall. A 20-mg sugar pellet was the natural food reward. Animals received a 3-sec, 20-Hz stimulation train with 5-ms pulses for optogenetic activation. Power output was adjusted to ~10 mW at the tip of the optic fiber under constant illumination. For all experiments, control mice were injected with AAV1-FLEX-mCherry.

Primary reinforcement for optical stimulation: Naïve animals were placed in the operant conditioning boxes for 1-hour sessions for 5 consecutive days. At baseline, both levers were

extended and the house light was illuminated. Each lever press (FR1, either lever) resulted in lever retraction, the house light turning off and a 3-sec train of optical stimulation at 20 Hz. 5 seconds following lever press/retraction, the levers re-extended and the house light was re-illuminated.

Primary reinforcement for food reward followed by optical stimulation: Naïve animals were placed in the operant conditioning boxes for 1-hour sessions for 10 consecutive days. At baseline, both levers were extended and the house light was illuminated. For the first 5 days of training, each lever press (FR1, either lever) resulted in immediate delivery of a 20 mg food pellet into the food hopper, in addition to lever retraction and the house light turning off. To promote learning of the contingency, the levers remained retracted and the house light off until a head entry into the food hopper was made. For training days 6 – 10, food pellet reward was exchanged for optical stimulation as above (FR1, either lever).

Primary reinforcement for food reward vs. optical stimulation: Animals underwent 3 days of instrumental conditioning for food pellet reward identical to the 1st 5 days of training above. Right and left lever presses were recorded. On the 4th day of training, one of the two levers was assigned to result in optical stimulation, while the other continued to result in food reward. This was counterbalanced to give equal lever presses on 'food-paired' and 'light-paired' levers prior to the transition on training day 4.

Progressive ratio: Animals that had previously learned to lever press for optical stimulation underwent an additional day of testing where the number of presses required to deliver optical stimulation increased non-arithmetically (i.e. 1, 2, 4, 6, 9, 13…) over the course of the session. The session ended after 3 consecutive minutes of no lever presses. Break point indicates the number of lever presses in the last successfully completed ratio.

Pavlovian conditioning followed by instrumental conditioning: Mice were bilaterally injected in the VTA with the red-shifted inhibitory opsin Jaws (AAV1-FLEX-Jaws-GFP). Bilateral cannulas were implanted 0.5 mm dorsal to the injection sites; one was lowered straight down while the other was implanted at a 10-degree angle. 3 seconds of optical inhibition (2 sec on with 1 sec ramp down) was delivered bilaterally through a split patch cable adjusted to give ~10 mW power at each optic fiber tip under constant illumination. Training sessions consisted of 25 trials in which 10-s lever extension (CS) was immediately followed by food pellet reward (US). Each trial was separated by a random inter-trial interval averaging 70 seconds and animals underwent 8 days of training. 3 seconds of optical inhibition began 100 ms prior to CS onset. A pulse (2 sec), ramp-down (1 sec) laser sequence was used to limit rebound excitation after laser-off. Head entries were recorded and quantified as a-per minute metric. After the 8 days of Pavlovian conditioning, mice were tested on an FR1 (food reward, either lever) task identical to primary reinforcement for food reward as above for 3 additional days.

Real-time place preference.: A custom made 2-chamber box was constructed with each chamber having unique contextual cues (horizontal vs. vertical wall stripes). A partial opening allowed free movement between the 2 chambers. On pre-test day 1, animals were attached to the patch cord and placed in the box for 10 minutes without any optical

stimulation. On subsequent days, the light-paired side was counterbalanced to account for any *a priori* preference. On test days 2 and 3, the light-paired side was paired with continuous optical excitation (ChR2: 20 Hz, 5-ms pulse width) or inhibition (Jaws: 2-sec pulse, 1-sec ramp down, 1 sec off) for the 20-minute session.

Quantification and Statistical Analysis.—Data were analyzed using GraphPad Prism version 6. For comparison of multiple treatments, a repeated measures one-way ANOVA with Tukey's post hoc multiple comparisons test between all groups was used (unless stated otherwise in the text). For analysis of experiments with multiple treatments and time-points, a two-way repeated measures ANOVA with Bonferonni's post hoc multiple comparisons test was used. Multiple comparisons correspond to time-points unless otherwise stated. Two-tailed student's t-test was used. All data were tested for normality and represented as mean +/− S.E.M..

Data and code availability

All data and custom software that support the current findings are available upon request from the Lead Contact, Larry Zweifel (larryz@uw.edu).

Supplementary Material

Refer to Web version on PubMed Central for supplementary material.

Acknowledgments

This work was supported by NIH grants P50-MH106428 (LSZ and CC), R01-MH104450 and R01-DA044315 (LSZ), 5T32AA007455-33 (GH), and the Howard Hughes Medical Institute (RDP). We thank Dr. Jeremy Clark for the use of voltammetry equipment, Dr. Sarah Ross for generously providing *Oprk1*-Cre mice, Dr. Martin Darvas for generously providing the Th^{lox} mice, Serina Tsang and Kathy Kafer for helping to generate new Cre-driver lines of mice, Dr. James Allen for assistance in AAV production, Dr. Scott Ng-Evans for software support, and members of the Zweifel lab for thoughtful discussion.

References

Berke JD (2018). What does dopamine mean? Nat. Neurosci 21, 787–793. [PubMed: 29760524]

Berridge KC, and Robinson TE (1998). What is the role of dopamine in reward: hedonic impact, reward learning, or incentive salience? Brain Res. Brain Res. Rev 28, 309–369. [PubMed: 9858756]

Bolam JP, and Smith Y (1990). The GABA and substance P input to dopaminergic neurones in the substantia nigra of the rat. Brain Res 529, 57–78. [PubMed: 1704287]

Borgland SL, Ungless MA, and Bonci A (2010). Convergent actions of orexin/hypocretin and CRF on dopamine neurons: Emerging players in addiction. Brain Res 1314, 139–144. [PubMed: 19891960]

Boyden ES, Zhang F, Bamberg E, Nagel G, and Deisseroth K (2005). Millisecond-timescale, genetically targeted optical control of neural activity. Nat. Neurosci 8, 1263–1268. [PubMed: 16116447]

Brown MT, Tan KR, O'Connor EC, Nikonenko I, Muller D, and Luscher C (2012). Ventral tegmental area GABA projections pause accumbal cholinergic interneurons to enhance associative learning. Nature 492, 452–456. [PubMed: 23178810]

Cai X, Huang H, Kuzirian MS, Snyder LM, Matsushita M, Lee MC, Ferguson C, Homanics GE, Barth AL, and Ross SE (2016). Generation of a KOR-Cre knockin mouse strain to study cells involved in kappa opioid signaling. Genesis 54, 29–37. [PubMed: 26575788]

Carter ME, Soden ME, Zweifel LS, and Palmiter RD (2013). Genetic identification of a neural circuit that suppresses appetite. Nature 503, 111–114. [PubMed: 24121436]

Chatterjee S, Sullivan HA, MacLennan BJ, Xu R, Hou Y, Lavin TK, Lea NE, Michalski JE, Babcock KR, Dietrich S, et al. (2018). Nontoxic, double-deletion-mutant rabies viral vectors for retrograde targeting of projection neurons. Nat. Neurosci 21, 638–646. [PubMed: 29507411]

Chung AS, Miller SM, Sun Y, Xu X, and Zweifel LS (2017). Sexual congruency in the connectome and translatome of VTA dopamine neurons. Sci. Rep 7, 11120. [PubMed: 28894175]

Chuong AS, Miri ML, Busskamp V, Matthews GA, Acker LC, Sorensen AT, Young A, Klapoetke NC, Henninger MA, Kodandaramaiah SB, et al. (2014). Noninvasive optical inhibition with a red-shifted microbial rhodopsin. Nat. Neurosci 17, 1123–1129. [PubMed: 24997763]

Clark JJ, Sandberg SG, Wanat MJ, Gan JO, Horne EA, Hart AS, Akers CA, Parker JG, Willuhn I, Martinez V, et al. (2010). Chronic microsensors for longitudinal, subsecond dopamine detection in behaving animals. Nat. Methods 7, 126–129. [PubMed: 20037591]

Cohen JY, Haesler S, Vong L, Lowell BB, and Uchida N (2012). Neuron-type-specific signals for reward and punishment in the ventral tegmental area. Nature 482, 85–88. [PubMed: 22258508]

Darvas M, Henschen CW, and Palmiter RD (2014). Contributions of signaling by dopamine neurons in dorsal striatum to cognitive behaviors corresponding to those observed in Parkinson's disease. Neurobiol. Dis 65, 112–123. [PubMed: 24491966]

Di Chiara G (2002). Nucleus accumbens shell and core dopamine: differential role in behavior and addiction. Behav. Brain Res 137, 75–114. [PubMed: 12445717]

Flagel SB, Clark JJ, Robinson TE, Mayo L, Czuj A, Willuhn I, Akers CA, Clinton SM, Phillips PE, and Akil H (2011). A selective role for dopamine in stimulus-reward learning. Nature 469, 53–57. [PubMed: 21150898]

Floresco SB (2015). The nucleus accumbens: an interface between cognition, emotion, and action. Ann. Rev. Psych 66, 25–52.

Grace AA, and Bunney BS (1984). The control of firing pattern in nigral dopamine neurons: burst firing. J. Neurosci 4, 2877–2890. [PubMed: 6150071]

Gore BB, Miller SM, Jo YS, Baird MA, Hoon M, Sanford CA, Hunker A, Lu W, Wong RO, and Zweifel LS (2017). Roundabout receptor 2 maintains inhibitory control of the adult midbrain. Elife 6.

Gore BB, and Zweifel LS (2013). Genetic reconstruction of dopamine D1 receptor signaling in the nucleus accumbens facilitates natural and drug reward responses. The J. Neurosci 33, 8640–8649. [PubMed: 23678109]

Gore BB, Soden ME, and Zweifel LS (2013). Manipulating gene expression in projection-specific neuronal populations using combinatorial viral approaches. Curr. Prot. Neurosci 65, 4 35 31–20.

Horvitz JC (2009). Stimulus-response and response-outcome learning mechanisms in the striatum. Behav. Brain Res 199, 129–140. [PubMed: 19135093]

Jo YS, Heymann G, and Zweifel LS (2018). Dopamine Neurons Reflect the Uncertainty in Fear Generalization. Neuron 100, 916–925 e913. [PubMed: 30318411]

Jo YS, and Mizumori SJ (2016). Prefrontal Regulation of Neuronal Activity in the Ventral Tegmental Area. Cereb. cortex 26, 4057–4068. [PubMed: 26400913]

Kalivas PW (1985). Interactions between neuropeptides and dopamine neurons in the ventromedial mesencephalon. Neurosci. Biobehav. Reviews 9, 573–587.

Kelley AE (1999). Functional specificity of ventral striatal compartments in appetitive behaviors. Ann. N. Y. Acad. Sci 877, 71–90. [PubMed: 10415644]

Kim J, Zhang X, Muralidhar S, LeBlanc SA, and Tonegawa S (2017). Basolateral to Central Amygdala Neural Circuits for Appetitive Behaviors. Neuron 93, 1464–1479 e1465. [PubMed: 28334609]

Kim JI, Ganesan S, Luo SX, Wu YW, Park E, Huang EJ, Chen L, and Ding JB (2015). Aldehyde dehydrogenase 1a1 mediates a GABA synthesis pathway in midbrain dopaminergic neurons. Science 350, 102–106. [PubMed: 26430123]

Lammel S, Hetzel A, Hackel O, Jones I, Liss B, and Roeper J (2008). Unique properties of mesoprefrontal neurons within a dual mesocorticolimbic dopamine system. Neuron 57, 760–773. [PubMed: 18341995]

Lein ES, Hawrylycz MJ, Ao N, Ayres M, Bensinger A, Bernard A, Boe AF, Boguski MS, Brockway KS, Byrnes EJ, et al. (2007). Genome-wide atlas of gene expression in the adult mouse brain. Nature 445, 168–176. [PubMed: 17151600]

Lima SQ, Hromadka T, Znamenskiy P, and Zador AM (2009). PINP: a new method of tagging neuronal populations for identification during in vivo electrophysiological recording. PloS one 4, e6099. [PubMed: 19584920]

Margolis EB, Hjelmstad GO, Fujita W, and Fields HL (2014). Direct bidirectional mu-opioid control of midbrain dopamine neurons. J. Neurosci 34, 14707–14716. [PubMed: 25355223]

Mohebi A, Pettibone JR, Hamid AA, Wong JT, Vinson LT, Patriarchi T, Tian L, Kennedy RT, and Berke JD (2019). Dissociable dopamine dynamics for learning and motivation. Nature 570, 65–70. [PubMed: 31118513]

Morales M, and Margolis EB (2017). Ventral tegmental area: cellular heterogeneity, connectivity and behaviour. Nat. Rev. Neurosci 18, 73–85. [PubMed: 28053327]

Parker JG, Zweifel LS, Clark JJ, Evans SB, Phillips PE, and Palmiter RD (2010). Absence of NMDA receptors in dopamine neurons attenuates dopamine release but not conditioned approach during Pavlovian conditioning. PNAS 107, 13491–13496. [PubMed: 20616081]

Patriarchi T, Cho JR, Merten K, Howe MW, Marley A, Xiong WH, Folk RW, Broussard GJ, Liang R, Jang MJ, et al. (2018). Ultrafast neuronal imaging of dopamine dynamics with designed genetically encoded sensors. Science 360.

Poulin JF, Caronia G, Hofer C, Cui Q, Helm B, Ramakrishnan C, Chan CS, Dombeck DA, Deisseroth K, and Awatramani R (2018). Mapping projections of molecularly defined dopamine neuron subtypes using intersectional genetic approaches. Nat. Neurosci

Qi J, Zhang S, Wang HL, Barker DJ, Miranda-Barrientos J, and Morales M (2016). VTA glutamatergic inputs to nucleus accumbens drive aversion by acting on GABAergic interneurons. Nat. Neurosci 19, 725–733. [PubMed: 27019014]

Saddoris MP, Cacciapaglia F, Wightman RM, and Carelli RM (2015). Differential Dopamine Release Dynamics in the Nucleus Accumbens Core and Shell Reveal Complementary Signals for Error Prediction and Incentive Motivation. J. Neurosci 35, 11572–11582. [PubMed: 26290234]

Saddoris MP, Sugam JA, Cacciapaglia F, and Carelli RM (2013). Rapid dopamine dynamics in the accumbens core and shell: learning and action. Front. Biosci 5, 273–288.

Sanford CA, Soden ME, Baird MA, Miller SM, Schulkin J, Palmiter RD, Clark M, and Zweifel LS (2017). A Central Amygdala CRF Circuit Facilitates Learning about Weak Threats. Neuron 93, 164–178. [PubMed: 28017470]

Saunders BT, Richard JM, Margolis EB, and Janak PH (2018). Dopamine neurons create Pavlovian conditioned stimuli with circuit-defined motivational properties. Nat. Neurosci 21, 1072–1083. [PubMed: 30038277]

Schultz W, Dayan P, and Montague PR (1997). A neural substrate of prediction and reward. Science 275, 1593–1599. [PubMed: 9054347]

Steinberg EE, Boivin JR, Saunders BT, Witten IB, Deisseroth K, and Janak PH (2014). Positive reinforcement mediated by midbrain dopamine neurons requires D1 and D2 receptor activation in the nucleus accumbens. PloS one 9, e94771. [PubMed: 24733061]

Stoeber M, Jullie D, Lobingier BT, Laeremans T, Steyaert J, Schiller PW, Manglik A, and von Zastrow M (2018). A Genetically Encoded Biosensor Reveals Location Bias of Opioid Drug Action. Neuron 98, 963–976 e965. [PubMed: 29754753]

Stuber GD, Hnasko TS, Britt JP, Edwards RH, and Bonci A (2010). Dopaminergic terminals in the nucleus accumbens but not the dorsal striatum corelease glutamate. J. Neurosci 30, 8229–8233. [PubMed: 20554874]

Taniguchi H, He M, Wu P, Kim S, Paik R, Sugino K, Kvitsiani D, Fu Y, Lu J, Lin Y, et al. (2011). A resource of Cre driver lines for genetic targeting of GABAergic neurons in cerebral cortex. Neuron 71, 995–1013. [PubMed: 21943598]

Ting JT, Daigle TL, Chen Q, and Feng G (2014). Acute brain slice methods for adult and aging animals: application of targeted patch clamp analysis and optogenetics. Methods Mol. Biol 1183, 221–242. [PubMed: 25023312]

Tritsch NX, Ding JB, and Sabatini BL (2012). Dopaminergic neurons inhibit striatal output through non-canonical release of GABA. Nature 490, 262–266. [PubMed: 23034651]

Tyree SM, and de Lecea L (2017). Lateral Hypothalamic Control of the Ventral Tegmental Area: Reward Evaluation and the Driving of Motivated Behavior. Front. Syst. Neurosci 11, 50. [PubMed: 28729827]

Valentino RJ, Reyes B, Van Bockstaele E, and Bangasser D (2012). Molecular and cellular sex differences at the intersection of stress and arousal. Neuropharmacology 62, 13–20. [PubMed: 21712048]

Wang F, Flanagan J, Su N, Wang LC, Bui S, Nielson A, Wu X, Vo HT, Ma XJ, and Luo Y (2012). RNAscope: a novel in situ RNA analysis platform for formalin-fixed, paraffin-embedded tissues. J. Mol. Diagn. JMD 14, 22–29. [PubMed: 22166544]

Werkman TR, McCreary AC, Kruse CG, and Wadman WJ (2011). NK3 receptors mediate an increase in firing rate of midbrain dopamine neurons of the rat and the guinea pig. Synapse 65, 814–826. [PubMed: 21218451]

Witten IB, Steinberg EE, Lee SY, Davidson TJ, Zalocusky KA, Brodsky M, Yizhar O, Cho SL, Gong S, Ramakrishnan C, et al. (2011). Recombinase-driver rat lines: tools, techniques, and optogenetic application to dopamine-mediated reinforcement. Neuron 72, 721–733. [PubMed: 22153370]

Yamaguchi H, Hopf FW, Li SB, and de Lecea L (2018). In vivo cell type-specific CRISPR knockdown of dopamine beta hydroxylase reduces locus coeruleus evoked wakefulness. Nat. Comm 9, 5211.

Yoo JH, Zell V, Gutierrez-Reed N, Wu J, Ressler R, Shenasa MA, Johnson AB, Fife KH, Faget L, and Hnasko TS (2016). Ventral tegmental area glutamate neurons co-release GABA and promote positive reinforcement. Nat. Comm 7, 13697.

Author Manuscript

Author Manuscript

Author Manuscript

Highlights

- Genetic isolation of projection-specific VTA neurons
- Differential role of VTA neurons in reward association and motivation
- Synergistic action of specialized VTA dopamine neurons for behavioral reinforcement

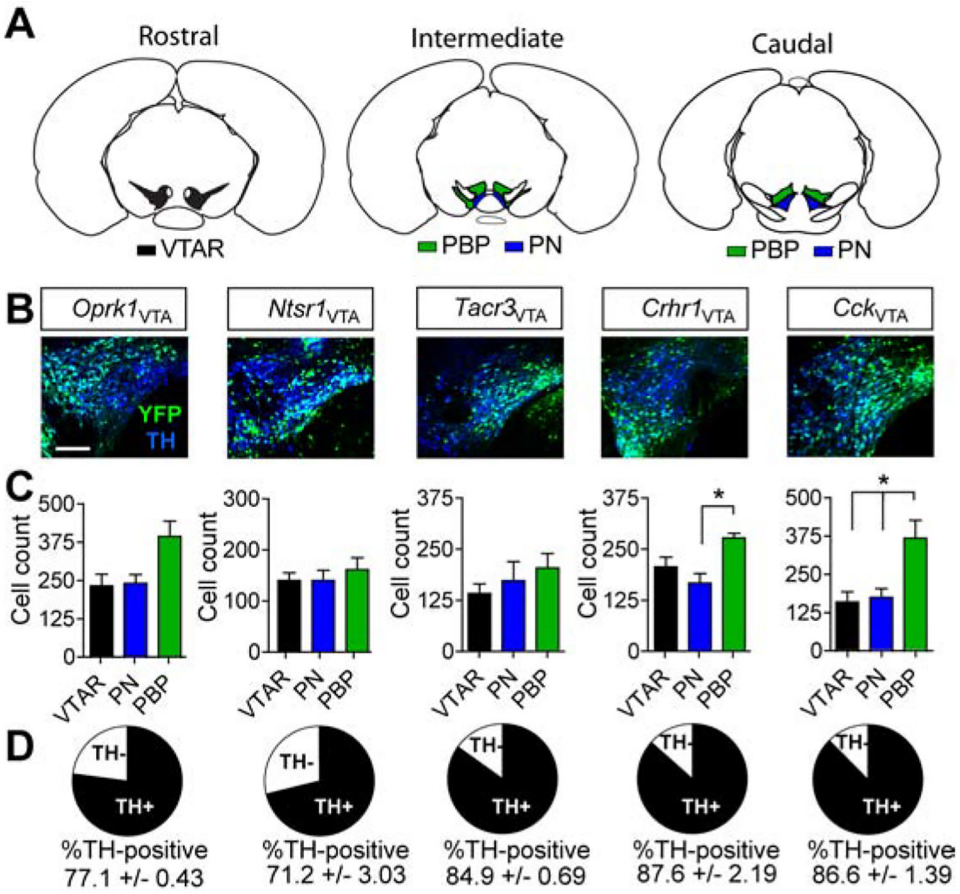

Figure 1. Genetic isolation of VTA sub-populations.

(A) Reference atlas images illustrating VTA subregions: rostral VTA (VTAR) – black; parabrachial pigmented nucleus (PBP) – green; paranigral nucleus (PN) – blue. (B) Example images of VTA sections co-stained for YFP (identifying VTA subpopulations after injection with AAV1-FLEX-YFP) and tyrosine hydroxylase (TH). Scale = 100μm. (C) Cell count quantification by VTA subregion (n=3 mice, 9 sections/animal; one-way ANOVA *Crhr1*: $F_{(2,8)}$=7.325, P<0.05; *Cck*: $F_{(2,8)}$=7.56, P<0.05, Tukey's multiple comparisons *P < .05). (D) Proportional overlap between YFP and TH. Data represented as mean +/− S.E.M.

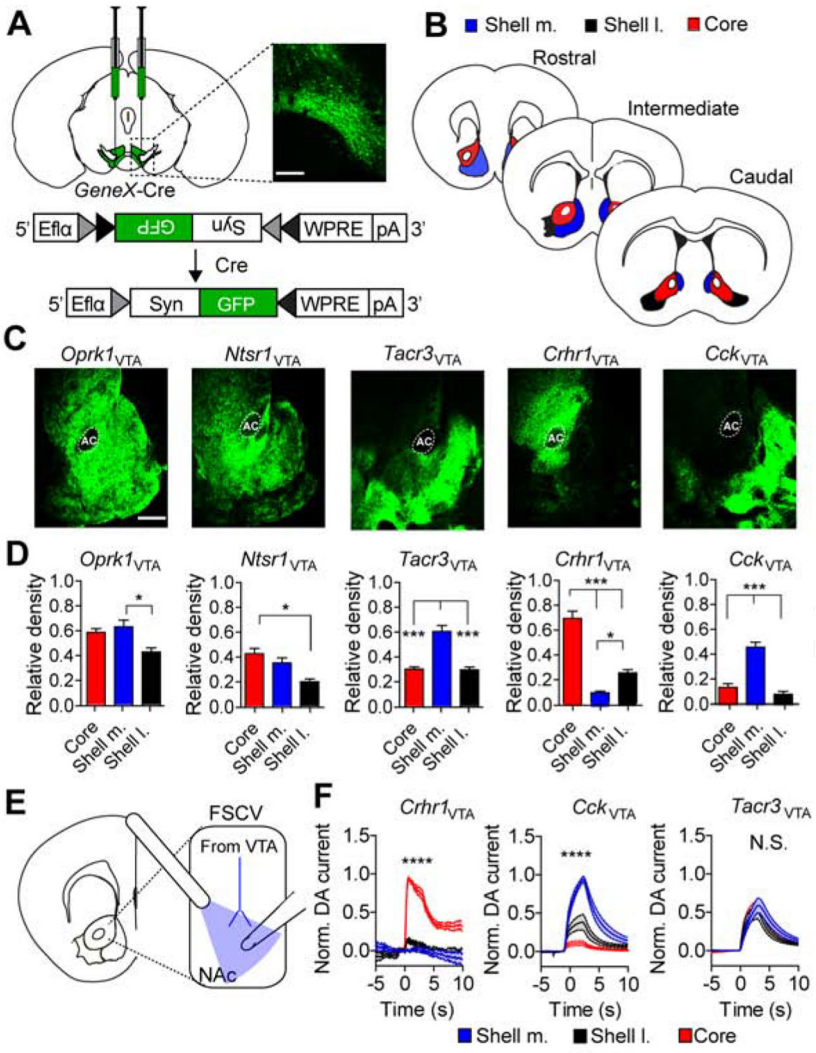

Figure 2. Segregated dopamine release and synaptic connectivity of isolated VTA neurons.

(A) Schematic of AAV-FLEX-Synaptophysin-GFP injection into VTA and corresponding histology image (scale = 250μm). (B) Illustration of subdivisions along the rostral, intermediate, and caudal extent of the NAc quantified in E. (C) Ventral striatal sections stained for synaptophysin-GFP (scale = 500μm). (D) Average pixel densities normalized to fluorescent intensity at the VTA injection site (*Oprk1* and *Ntsr1*: n=3 mice, 9 sections; *Tacr3*: n=4 mice, 12 sections; *Crhr1* and *Cck*: n=5 mice, 14–15 sections; one-way ANOVA *Oprk1*: $F_{(2,8)}$=7.074, P<0.05; *Ntsr1*: $F_{(2,8)}$=9.912, P<0.05; *Tacr3*: $F_{(2,9)}$=28.2, P<0.001; *Crhr1*: $F_{(2,12)}$=67.84, P<0.0001; *Cck*: $F_{(2,12)}$=19.64, P<0.0001, Tukey's multiple comparisons *P<0.05, **P<0.01, ***P<0.001, ****P<0.0001). (E) Illustration of slice voltammetry for recording optically-evoked dopamine release in NAc subregions. (F) Normalized dopamine current evoked by 3 seconds of 20-Hz optical stimulation of $Crhr1_{VTA}$, Cck_{VTA} and $Tacr3_{VTA}$ ChR2-expressing terminals. Recordings from all 3 subregions were taken for each slice and normalized to the peak current amplitude per slice (*Crhr1*: n=4 mice, 9 sections; *Cck*: n=4 mice, 8 sections; *Tacr3*: n=4 mice, 15 sections, , two-

way ANOVA *Crhr1*: $F_{(298,3576)}$=27.23, P<0.0001; *Cck*: $F_{(298,2100)}$=11.64, P<0.0001, Bonferroni multiple comparisons ****P<0.0001).

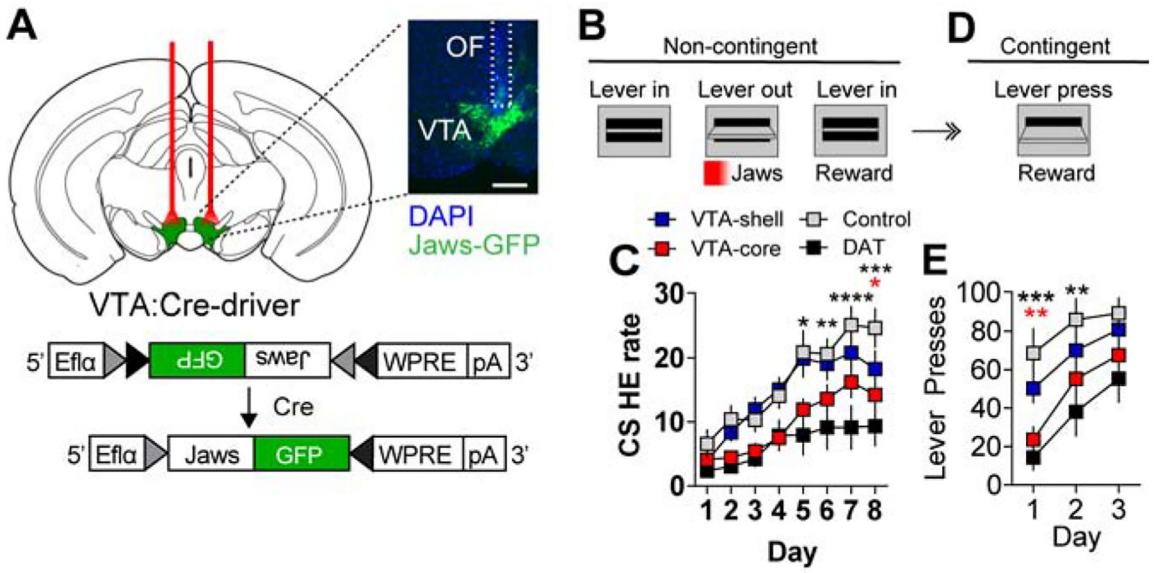

Figure 3. Differential dependence of *Crhr1*$_{VTA}$ and *Cck*$_{VTA}$ neurons for Pavlovian association.

(A) Schematic of AAV1-FLEX-Jaws-GFP expression and bilateral optical cannulation in the VTA to inhibit *Crhr1*$_{VTA}$, *Cck*$_{VTA}$, or DAT$_{VTA}$ neurons (scale = 500μm). (B) During Pavlovian conditioning optogenetic inhibition was paired with CS onset. Each 10-s CS presentation was immediately followed by food pellet delivery. (C) Head-entry rate (per min) into the food hopper during 10-s CS presentation over 8 days of conditioning (*Crhr1*$_{VTA}$ and *Cck*$_{VTA}$: n=12 mice/group, Control (GFP): n=11, DAT$_{VTA}$: n=9; Two-way ANOVA $F_{(21,280)}$=1.97, P<0.01, Bonferroni multiple comparisons *P<0.05, **P<0.01). (D) Schematic for FR1 instrumental conditioning following 8 days of Pavlovian conditioning. (E) Lever presses/day over 3 days of instrumental conditioning Two-way ANOVA $F_{(3,40)}$=8.53, P<0.001, Bonferroni selected comparisons to controls *P<0.05, ***P<0.001). In C and E the black stars represent DAT-Cre mice compared to controls and the red stars represent *Crhr1*-Cre mice compared to controls.

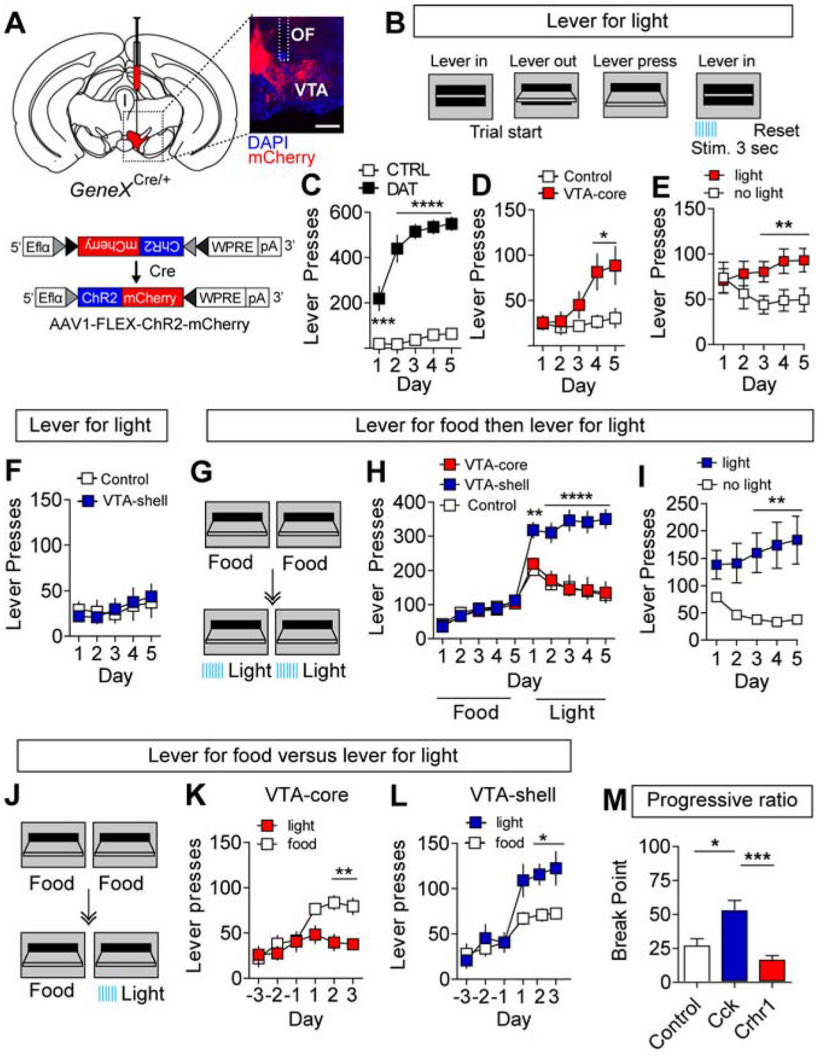

Figure 4. *Crhr1*$_{VTA}$ and *Cck*$_{VTA}$ neurons are operationally distinct.

(A) Schematic of AAV1-FLEX-ChR2-mCherry injected into the VTA of Cre-driver lines and representative immunohistochemical staining (optic fiber placement — white dashed lines, scale = 500μm). (B) Schematic of instrumental conditioning paradigm for optical stimulation. Each lever press resulted in immediate stimulation (3 s, 20 Hz, 5-ms pulse width) and a 5-s timeout before lever re-extension. (C) Lever presses/day for stimulation of dopamine neurons in DAT-Cre mice (Control n=6, DAT-Cre n=6, Two-way repeated measures ANOVA, $F_{(4,10)}$=38.16, P<0.0001 Bonferroni multiple comparisons, ***P<0.001, ****P<0.0001). (D) Lever presses/day for VTA-Core projecting mice expressing ChR2-mCherry (n=9) or mCherry (control, n=6; Two-way repeated measures ANOVA, $F_{(4,52)}$=4.461, P<0.01 followed by Bonferroni multiple comparisons, *P<0.05). (E) Lever presses on active (previously non-preferred lever) and inactive (previously preferred lever) in VTA-Core projecting mice expressing ChR2-mCherry (n=8; Two-way repeated measures ANOVA, $F_{(4,56)}$=4.52, P<0.01 followed by Bonferroni multiple comparisons, **P<0.01; Note, one *Crhr1*-Cre mouse expressing ChR2-mCherry did not lever press and was not assayed on the switching assay). (F) Lever presses/day for VTA-Shell projecting mice

expressing ChR2-mCherry (n=9) or mCherry (n=8). (G) Schematic illustrating 5 days of instrumental conditioning for food reward followed by 5 days for ICOSS. (H) Lever presses/day for VTA-core, VTA-shell, and control groups (VTA-Core and control: n=8 mice, VTA-shell: n=7 mice two-way ANOVA $F_{(18,180)}$=11.46, P<0.0001, Bonferroni multiple comparisons, **P< 0.01, ****P<0.0001). (I) Lever presses on active (previously non-preferred lever) and inactive (previously preferred lever) in VTA-shell mice expressing ChR2-mCherry (n=7, two-way repeated measures ANOVA, $F_{(4,48)}$=9.87, P<0.0001 followed by Bonferroni multiple comparisons, **P<0.01). (J) Schematic of food reward vs. optogenetic stimulation paradigm (left). Mice underwent 3 days (days −3 through −1) of FR1 instrumental conditioning for food reward. On days 1 through 3, one lever was switched to give light stimulation (3 s, 20 Hz, 5-ms pulse width). (K-L) VTA-core (K) and VTA-shell (L) lever presses/day on food- and light-paired levers (VTA-Core: n=6 mice; VTA-shell: n=8 mice; two-way ANOVA VTA-Core: $F_{(5,50)}$=5.37, P<0.001; VTA-shell: $F_{(5,70)}$=4.97, P<0.001, Bonferroni multiple comparisons, *P< 0.05, **P<0.001). (M) Average break points on progressive ratio task (control: n=18 mice; VTA-shell: n=16 mice; VTA-Core: n=17 mice; one-way ANOVA $F_{(4,54)}$=6.481, P<0.001, Bonferroni multiple comparisons, *P<0.05, **P<0.001).

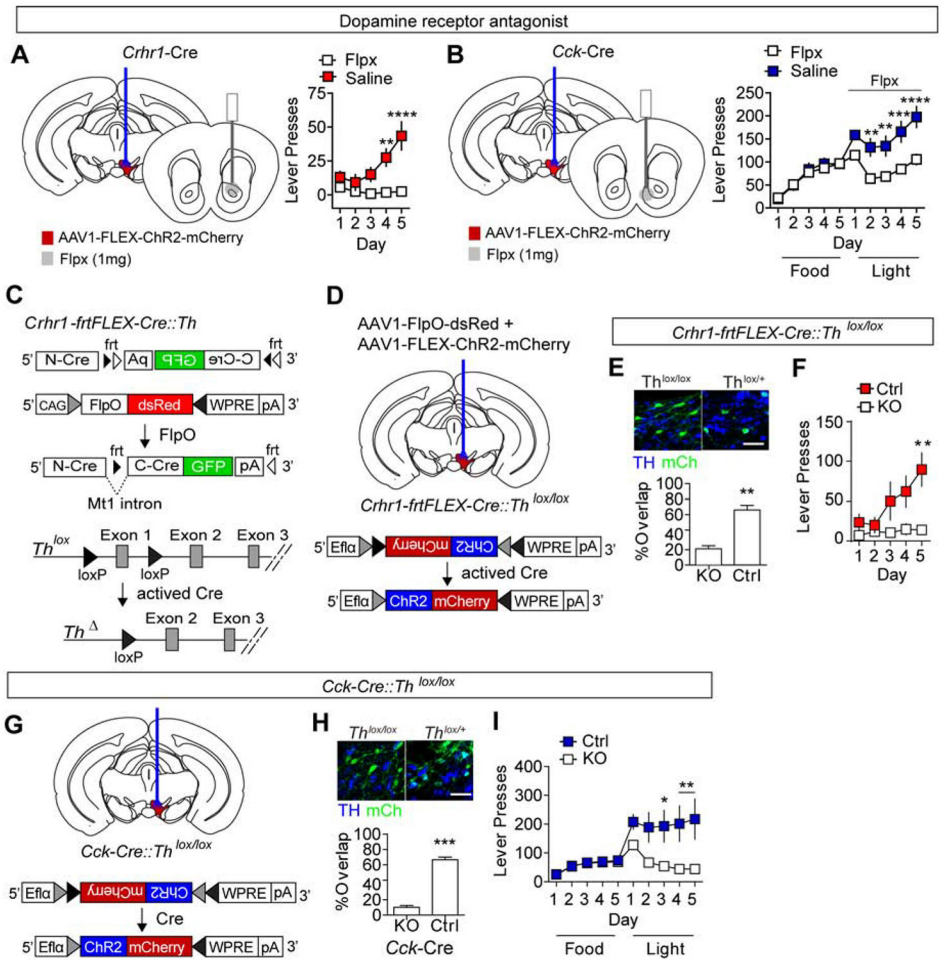

Figure 5. Dopamine dependence of behavioral regulation.

(A-B) Infusion of dopamine receptor antagonist Flpx (1μg) into the NAc Core (A) or NAc Shell (B) blocks the effects of ICOSS in VTA-Core or VTA-shell mice, respectively (VTA-core, n=7 mice/group, two-way ANOVA $F_{(4,48)}$=10.90, P<0.0001, Bonferroni multiple comparisons **P<0.01, ****P<0.0001; VTA-shell, n=7 mice/group, two-way ANOVA $F_{(9,108)}$=7.37, P<0.0001, Bonferroni multiple comparisons **P<0.01, ****P<0.0001). (C) Schematic illustration of frtFLEX-Cre. The C-terminus of split Cre is inverted relative to the N-terminus and flanked by inverted non-homologous frt sites (frt1 and frt5). Viral expression of FlpO inverts the C-terminus and a metalothionine 1 (*Mt1*) intron facilitates splicing. Following Cre activation the first exon of *Th* is removed (Th^{Δ}) resulting in gene inactivation. (D) Co-injection of AAV1-FlpO-dsRed and AAV1-FLEX-ChR2-mCherry in to in *Crhr1-frtFLEX*-Cre::$Th^{lox/lox}$ or *Crhr1-frtFLEX*-Cre::$Th^{lox/+}$ mice allows for *Th* inactivation and ChR2 expression. (E) Co-staining for TH and ChR2-mCherry in *Crhr1-frtFLEX*-Cre::$Th^{lox/lox}$ or *Crhr1-frtFLEX*-Cre::$Th^{lox/+}$ mice (% overlap of mCherry and TH, n=3 mice, 2–4 sections/animal, unpaired student's t-test t=7.156, **P<0.01). Note: mCherry is pseudo-colored green for ease of visualization, scale = 25μm. (F) Lever presses/day during FR1 for optogenetic stimulation conditioning paradigm (n=7 mice/group, two-way ANOVA $F_{(4,48)}$=3.34, P<0.05, Bonferroni multiple comparisons P<0.01). (G) Schematic illustration of AAV1-FLEX-ChR2-mCherry injection and optical cannulation of *Cck-*

Cre::Th$^{lox/lox}$ mice. (H) Co-staining for TH (blue) and mCherry (green) in *Cck*-Cre::*Th*$^{lox/lox}$ or *Cck*-Cre::*Th*$^{lox/+}$ mice injected with AAV1-FLEX-ChR2-mCherry (% overlap of mCherry and TH, n=3 mice, 2–4 sections/animal, unpaired student's t-test t=14.45, ***P<0.001). Note: mCherry is pseudo-colored green for ease of visualization, scale = 25μm. (I) Lever presses/day during FR1 for food reward followed by FR1 for optogenetic stimulation conditioning paradigm (lox/+: n=7mice; lox/lox: n=6 mice, two-way ANOVA $F_{(9,99)}$=4.19, P<0.0001, Bonferroni multiple comparisons *P<0.05, **P<0.01).

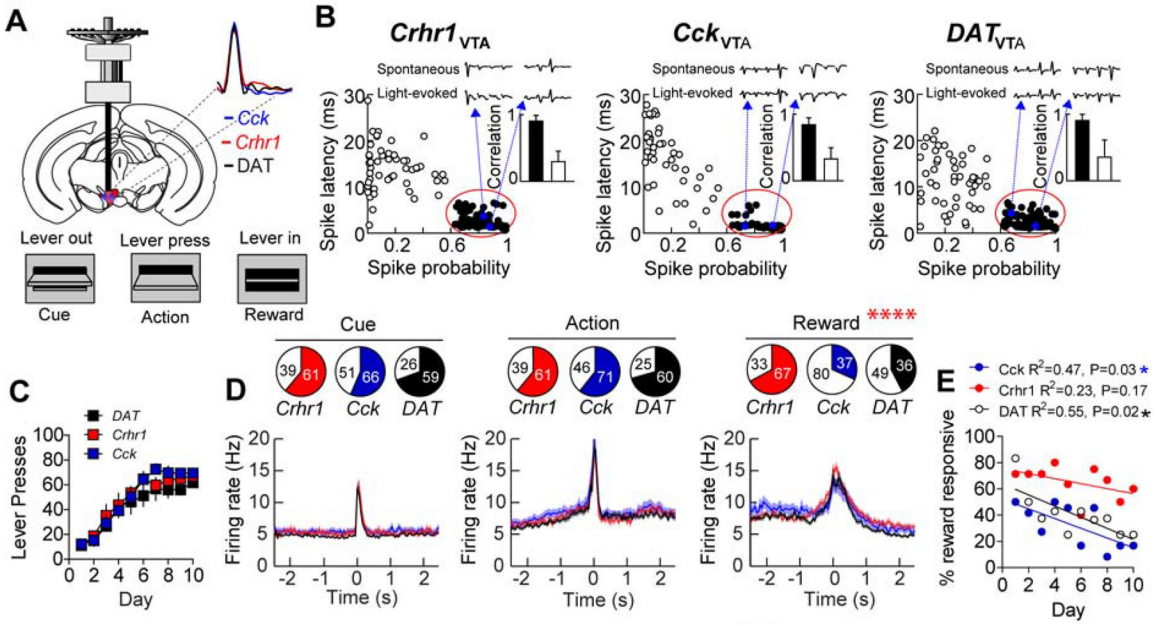

Figure 6. Reward encoding by *Crhr1*$_{VTA}$ and *Cck*$_{VTA}$ populations.

(A) Schematic of recording paradigm. Inset: average waveforms of optically-sensitive neurons from *Crhr1*-, *Cck*-, and DAT-Cre mice. (B) Optical identification of ChR3-expressing neurons during *in vivo* tetrode recording. Neurons with short-latency, high-fidelity responses to light (filled circles) were characterized as optically sensitive. Inset: action potential waveform correlations between light-evoked and spontaneous action potentials (black bars are light-sensitive units, white bars are light-insensitive units). (C) Lever presses over the one-hour conditioning sessions during recording days. (D) Proportion of responsive cells to each of the three events and corresponding time-locked activity in these responsive cells from *Crhr1*-Cre: n=4 mice, *Cck*-Cre: n=3 mice, and DAT-Cre n=3 mice. Proportion of reward responsive cells, P<0.0001, *Chi*-square$_{(2)}$=27.90. (E) Proportion of cells responding to reward across days of conditioning (Pearson r, *P<0.05)

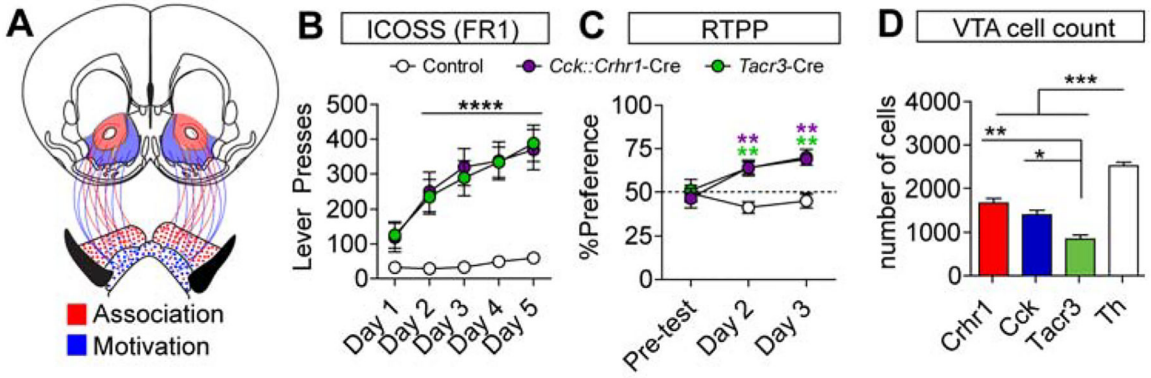

Figure 7. Cooperativity of VTA subpopulations maximizes reward reinforcement.

(A) Circuit model demonstrating dissociable VTA projections (VTA-core, red; VTA-shell, blue) and reward processes. (B) Lever presses/day for ICOSS over 5 FR1 instrumental conditioning days for double transgenic *Crhr1*-Cre::*Cck*-Cre (VTA-core::VTA-shell) mice and *Tacr3*-Cre mice (*Tacr3*-Cre: n=6 mice and *Crhr1*-Cre*::Cck*-Cre: n=7 mice). (C) Time spent in light-paired chamber (20 Hz, 5ms pulse width) during RTPP assay. Mice underwent a 10 minute pre-test on day 1, followed by light pairing for 20 minutes on days 2 and 3, analysis was performed in 5 min bins (AAV1-FLEX-mCherry control: n=10 mice; DAT-Cre: n=7 mice; *Crhr1*-Cre: n=9 mice; *Cck*-Cre: n=14 mice; *Crhr1*-Cre::*Cck*-Cre: n=7 mice; *Tacr3*-Cre: n=6 mice, two-way ANOVA $F_{(4,34)}$=6.2, P=0.0007; Bonferroni multiple comparisons to **P<0.01 relative to controls). (D) Total VTA cell counts (n=3 mice/group, *Crhr1*-Cre, *Cck*-Cre, and *Tacr3*-Cre, n=9 combined TH counts, one-way ANOVA ANOVA $F_{(3,17)}$=52.19, P<0.0001; Tukey's multiple comparisons *P<.05, **P<.01, ****P<0.0001).

Additional Resources

REAGENT or RESOURCE	SOURCE	IDENTIFIER
Antibodies		
anti-tyrosine hydroxylase	Millipore	MAB318
anti-tyrosine hydroxylase	Millipore	AB152
anti-dsRed	Clontech	632496
anti-GFP	Millipore	MAB3580
Secondary antibodies conjugated with AlexaFluor 488 or Cy3	Jackson Immunoresearch	
Bacterial and Virus Strains		
AAV- Ef1α-FLEX-ChR2-mCherry	University of Washington	N/A
AAV-CAG-FLEX-Jaws-GFP	University of Washington	N/A
pAAV- Ef1α-FLEX-mCherry	University of Washington	N/A
pAAV- Ef1α-FLEX-YFP	University of Washington	N/A
pAAV-CAG-FlpO-dsRed	University of Washington	N/A
Experimental Models: Organisms/Strains		
Slc6a3$^{Cre/+}$ (DAT-Cre) mice	Jackson laboratory	20080
Cck$^{Cre/+}$ mice	Jackson laboratory	012706
Oprk1$^{Cre/+}$ *mice*	University of Pittsburgh	N/A
Th$^{lox/lox}$	University of Washington	N/A
Crhr1$^{Cre/+}$	University of Washington	N/A
Crhr1$^{frtFLEX\text{-}Cre/+}$	University of Washington	N/A
Ntsr1$^{frtFLEX\text{-}Cre/+}$	University of Washington	N/A
Tacr3$^{Cre/+}$	University of Washington	N/A
Software and Algorithms		
Offline sorter for cluster cutting	Plexon	v3.3.5
Ethovision for tracking mice movement	Noldus	XT8.5
Matlab script for data analysis	Yong Sang Jo	N/A
Med Associates scripts for appetitive behavior	Scott Ng-Evans	N/A